

Dynamic calibration of force balances for impulse hypersonic facilities

David J. Mee

Centre for Hypersonics, The University of Queensland, Brisbane. 4072. Australia.

Received: 17 May 2002 / Accepted: 11 December 2002

Abstract. This paper analyzes different techniques for the calibration of force balances for use in short-duration impulse hypersonic facilities such as shock tunnels. The background to how deconvolution can be used to infer aerodynamic forces on models in impulse hypersonic wind tunnels is presented along with the theory behind the different calibration techniques. Four calibration techniques are applied to a single-component stress-wave force balance. Experiments in the T4 shock tunnel using the balance demonstrate the suitability of the different calibrations for force measurements in an impulse facility. Cross checks between the calibration techniques are used to check their ranges of validity. It is shown that the impulse response derived from tests in which the model and force balance are suspended from a fine wire and the wire cut agree well with impulse responses derived from calibrations made using an impact hammer. The suitability of the balance for measuring dynamic forces is demonstrated by showing that the drag force on a model follows the history of Pitot pressure in the test section in the tunnel shots.

Key words: Force balance, Shock tunnel, Calibration, Deconvolution

PACS codes: 47.40.Ki, 47.80.+v, 07.10.Pz

1 Introduction

The measurement of aerodynamic forces on models in hypersonic impulse facilities has been restricted in the past because of the time it takes for the test model to reach a state of force equilibrium with its support mechanisms (Bernstein, 1975). Conventional force balances rely on damping mechanisms and/or filters to reduce the effects of vibrations, associated with the sudden application of aerodynamic forces when the flow starts or when the model is injected into the flow. In impulse facilities, particularly high-enthalpy facilities, the duration of the test flow may be insufficient for such vibrations to be damped before the end of the test. The period of vibrations can even exceed the test time.

Various techniques can be used to address these problems. The model can be made small and light and the force balance very stiff so that the natural frequency of the system is high (e.g. Jessen and Groenig, 1989). Accelerometers can be placed on the model and can be used to detect vibrations that can then be used to compensate the strain signals from the force balance (e.g. Carbonaro, 1993). Another possibility is to measure the acceleration of the model and use flexible supports for the model (e.g. Joshi and Reddy, 1986) or to let the model fly freely during the test (e.g. Naumann *et al.*, 1993). This eliminates the effect of a support mechanism decreasing the natural frequencies of the system. The natural frequencies are set by the model size and the speed of stress

waves in the structure of the model. A small model keeps these frequencies high and a light model leads to larger acceleration signals.

When force measurements are required on models of larger size and mass in impulse facilities, the period of the lowest natural frequency of the force balance can become of similar order to the duration of the test flow. For such conditions, system identification and inverse techniques can be used. The system dynamics can then be included in the analysis of the force balance signals to determine the history of the aerodynamic forces on the model. One such technique, the stress-wave force balance (SWFB) technique, was proposed by Sanderson and Simons (1991). This technique has been extended to larger sized models (Tuttle *et al.*, 1995), shorter duration flows (Smith and Mee, 1996a), multiple-component force measurement (Mee *et al.*, 1996) and has been used for measurements such as the performance of scramjet-powered vehicles (Paull *et al.*, 1995). An overview of dynamic testing is given by McConnell (1995) and the dynamic calibration of measurement systems is discussed by McConnell and Abdelhamid (1987).

This paper presents four techniques that can be used to determine the impulse response for force balances for use in impulse hypersonic facilities. The background behind the calibration techniques is presented in sections 2 and 3. A single-component force balance (a drag balance) is considered in section 4. The results from the four calibration techniques are discussed and comparisons between

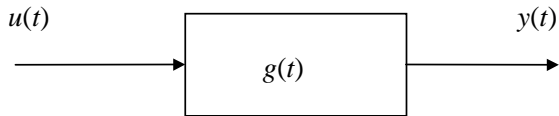


Fig. 1. Schematic of a linear system representing a force-wave force-balance

them are made. The results from experiments using the balance in the T4 free-piston shock tunnel are then presented and results of using the different calibration techniques are compared.

2 Dynamics of force balances

When an aerodynamic load is suddenly applied to a model in the test section of an impulse facility, stress waves are initiated within the model. These stress waves propagate and reflect within the model and its support structure. During the short period of steady flow, no steady state of force equilibrium can be achieved between the model and its support. By taking into account the dynamics of the model and force balance arrangement, the history of the aerodynamic forces on the model which caused the stress wave activity can be determined from the measurement of the strain histories (at one or more locations on the model or its support structure).

The aerodynamic model and its support structure behave as a linear dynamic system for forces which lead to linear strains. Such a linear system is shown schematically in Fig. 1 and can be represented by the convolution integral,

$$y(t) = \int_0^t g(t - \tau)u(\tau) d\tau. \quad (1)$$

For a SWFB, $u(t)$ is the applied load, $y(t)$ is the strain measured at some point on the structure and $g(t)$ is the impulse response function.

If the system characteristics (in the form of the impulse response function) are known, then a deconvolution procedure can be used to determine the history of the applied load from the history of measured strain.

3 Theoretical background

3.1 Determination of the impulse response from a step input

One method for experimentally determining the impulse response is to measure the output signal generated by a step change in the input to the system. This is called the step response of the system. The impulse response can be determined by differentiating the step response with respect to time and scaling the result appropriately. This

can be shown by taking the Laplace transform of eq. (1) to obtain

$$Y(s) = G(s)U(s), \quad (2)$$

where $Y(s)$, $G(s)$ and $U(s)$ are the Laplace transforms of $y(t)$, $g(t)$ and $u(t)$ respectively. Let the input be a step of magnitude a starting at time $t = 0$,

$$u(t) = \begin{cases} 0 & t < 0, \\ a & t \geq 0. \end{cases} \quad (3)$$

The Laplace transform of this input is a/s and eq. (2) becomes

$$Y(s) = \frac{aG(s)}{s} \quad (4)$$

Inverting this gives

$$y(t) = a \int_0^t g(\tau) d\tau, \quad (5)$$

or

$$g(t) = \frac{1}{a} \frac{dy(t)}{dt}. \quad (6)$$

Therefore the impulse response can be determined from the response of the system to a step of magnitude a .

The ideal step response excites all frequencies of the system. However the amplitudes of excitation are heavily weighted to low frequencies (Reed, 1998). This can be seen by noting that the amplitudes of the sinusoidal Fourier components that go to make up a step have amplitudes that vary inversely with frequency. As noted by Reed (1998), “While complete representation of the ideal step also requires all frequencies, the amplitudes at the higher frequencies rapidly become infinitesimal, therefore negligible.”

If a finite element model of the SWFB arrangement is made, step responses can be determined by dynamic analysis. This has been used extensively at The University of Queensland for designing a SWFB (Daniel and Mee, 1995; Smith *et al.*, 2001). In some cases impulse responses derived by differentiating step responses obtained using finite element analysis have been used to deconvolve wind tunnel data (Sanderson and Simmons, 1991; Smith and Mee, 1996a). In order to avoid any errors due to modelling approximations used in the finite element analysis, it is preferable to measure the step response experimentally.

To demonstrate how a step response can be obtained experimentally, consider a single-component SWFB, such as that of Sanderson and Simmons (1991), consisting of an axisymmetric model attached to a long stress bar aligned with the axis of the model (Fig. 2). An approximate step change in axial load on the model can be applied by attaching a fine wire to the tip of the model, applying a load to it, and then cutting the wire. This requires the right hand end of the stress bar (in Fig. 2) to be held so that free-body motion of the arrangement does not occur when the load is applied via the wire. Two possible calibration arrangements are shown in Figs. 3 and 4(a) where a known mass is attached to the wire to apply a known

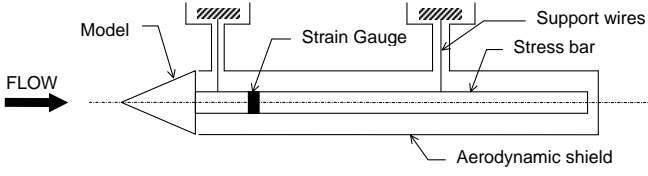


Fig. 2. Single-component stress-wave force-balance

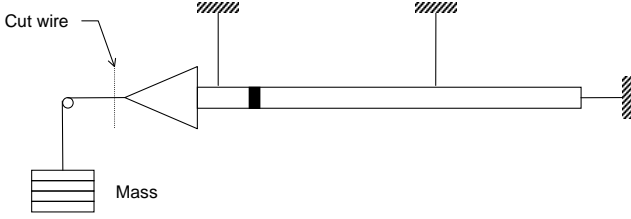
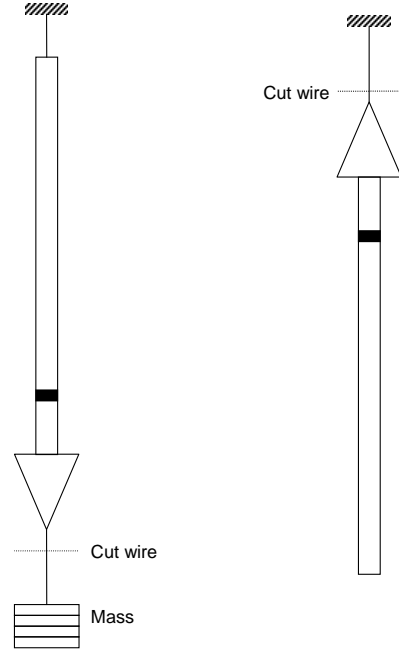


Fig. 3. Horizontal Calibration

load to the model. In Fig. 3, the model is supported horizontally (as it is in the test section of the wind tunnel) and the wire passes over a pulley to the mass. The wire is cut close to the model. In Fig. 4(a), the axis of the balance is vertical and the balance is supported by a wire attached to the end of the stress bar. Each of these techniques has been used to obtain step responses.

Similar calibration techniques can also be used for force balances where the end of the sting is rigidly fixed (e.g. Smith *et al.*, 2001). If the calibrations are done when the model is mounted in the tunnel, then the characteristics of the tunnel mounting arrangement are included in the derived impulse response. However, for balances where the downstream end of the stress bar is free (as in Fig. 2), calibrations using the arrangements in Figs. 3 and 4(a) can be inadequate. The impulse response derived from a step response for one of these arrangements will only be valid for the period of time it takes for a stress wave to travel from the tip of the model, reflect from the end of the stress bar and return to the strain measurement location. (For a 300 mm aluminium model, a 2 m brass stress bar and the strain gauge located on the brass bar 200 mm from the model, this time would be 1.15 ms.) Thus the maximum length of tunnel signal that could be processed with such an impulse response would be limited to this time.

This deficiency can be overcome by the calibration arrangement shown in Fig. 4(b). Here the SWFB is again supported vertically but the load applied to the tip of the model is the weight of the SWFB and the end of the stress bar is free. When the wire is cut, the load is suddenly removed at the tip and the arrangement falls. During the period of free-fall there is no load on the model and a step response, valid for the tunnel experiments, is obtained for a longer period of time. The magnitude of the applied step is set by the mass of the model and stress bar.



(a) Vertical calibration. (b) Free-end calibration.

Fig. 4. Vertical calibration techniques.

3.2 Determination of the impulse response from a pulse test

Another method for determining the impulse response is to apply an impulse to the system and to measure the response of the system. This is an attractive method for exciting the system because a true impulse (delta function or Dirac function) is equivalent to applying the set of all harmonic functions simultaneously for all frequencies (Dieulesaint and Royer, 1980, pp. 28–29). Thus, this method can potentially provide as much information as a point-by-point analysis for every frequency. Of course, there are practical limitations to this, as discussed below.

Consider an input to the system which has the form of a perfect impulse, i.e. $u(t) = S\delta(t)$ where $\delta(t)$ is the unit impulse function,

$$\delta(t) = \begin{cases} 0 & t \neq 0, \\ \infty & t = 0, \end{cases} \quad (7)$$

with

$$\lim_{\epsilon \rightarrow 0} \int_{-\epsilon}^{+\epsilon} \delta(t) dt = 1$$

and S is the time integral of the pulse. Then from eq. (1)

$$y(t) = \int_0^t g(t - \tau) S \delta(\tau) d\tau. \quad (8)$$

Since the convolution integral is commutable, this can be rewritten as

$$y(t) = \int_0^t g(\tau) S \delta(t - \tau) d\tau = S \int_0^t g(\tau) \delta(t - \tau) d\tau. \quad (9)$$

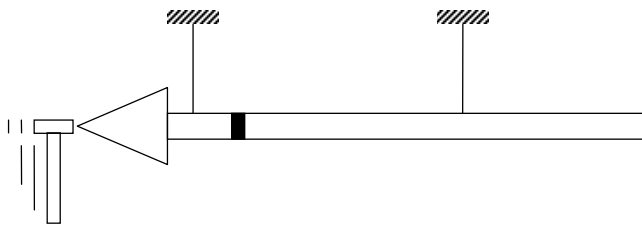


Fig. 5. Pulse Calibration

Noting the shifting property of the delta function,

$$\int_0^t f(\tau)\delta(t - \tau) d\tau = f(t), \quad (10)$$

the final result is

$$y(t) = Sg(t). \quad (11)$$

Thus the response to a perfect impulse of area S is the true impulse response scaled in magnitude by S .

A perfect impulse cannot be achieved in practice and the question which arises is how short or sharp does an impulse need to be in order to produce essentially the same response as the perfect impulse. The relevant timescale is the characteristic time of the system under test. As demonstrated in Doebelin (1980), when the period of the pulse is short in comparison with the characteristic time of the system, the details of the shape of the pulse make no difference to the response obtained and only the area of the pulse is important. When the period of the pulse is not short, the response is dependent on the shape of the pulse.

One technique for calibrating a SWFB is to apply a short force pulse at a point on the model using an instrumented impactor. Such an arrangement is shown schematically in Fig. 5. The impactor, shown as a hammer, is instrumented to indicate the history of force applied during the pulse. If the period of the pulse is short in comparison with the characteristic time for the balance and the magnitude of the pulse is measured, the impulse response can be determined from the system response using eq. (11). Another possibility is to use a pendulous mass as an impactor and to determine the impulse applied from the velocities of the mass immediately before and after impact (Mee, 2002).

3.3 Determination of the impulse response by measuring the response to an arbitrary input

Equation (1) indicates that the relationship between an input $u(t)$ and the associated output $y(t)$ is in the form of a convolution integral. This suggests that by applying any measurable transient input to the system and measuring the response, deconvolution techniques could be used to determine the impulse response, $g(t)$.

There is a limitation to this method that can be explained in terms of the frequency spectra of the input to the system and the impulse response. There is a loss

of accuracy in applying deconvolution techniques at frequencies where the impulse response is non-zero but the applied input is small. At such frequencies any measurement or digitization errors in the input or output can lead to an unreliable impulse response being calculated. Thus the frequency content of the input and impulse response must be considered when trying to determine $g(t)$ from an arbitrary input. An input signal that has a shape similar to that expected in an experiment should be suitable for calibration. However, it is not necessary to have the same time record for the calibration input and the experiment input in order for deconvolution to be successful.

One type of input that could be used to determine the impulse response by deconvolving the output signal with the input signal is the pulse input discussed in section 3.2. Instead of dividing the response by the impulse applied, as discussed in section 3.2, the shape of the pulse could be measured as well as its magnitude. Then the measured input pulse signal could be used to deconvolve the measured output signal to infer the impulse response. A pulse input does not resemble the force history on a model in a hypersonic impulse facility. However, it is shown in section 4 that this can lead to a good estimate of the system impulse response. Such a calibration technique can potentially provide details of the impulse response for higher frequencies than can the method of simply dividing the balance response by the magnitude of the applied impulse. This is because the shape of the pulse can be taken into account.

4 Experiments

A single-component stress-wave force balance for measurement of the drag force on a sharp cone has been used to demonstrate the calibration techniques outlined in section 3. The balance was used to measure drag forces on the cone when it was exposed to flow in the test section of the T4 free-piston shock tunnel. Calibration tests were performed on the force balance both when it was outside and inside the tunnel.

The model used was a sharp cone of 15° semi-angle and 182 mm axial length. The body of the cone was made from aluminium and it had a stainless steel tip. The cone was mounted on a tubular brass stress bar of 2.4 m length, 35 mm outer diameter and 1.7 mm wall thickness. For the pulse calibration tests and the tunnel tests, the complete model was suspended by two fine wires, as in Fig. 2. There were two steel tips for the model; one was a sharp, 18 mm long, conical tip and the other was a cylindrical tip, 25 mm long and 13 mm in diameter with a flat end. The cylindrical tip was used to apply loads in the calibration tests. For the calibration tests in which either the model was suspended on a fine wire or a weight was attached to the model via a wire (see Fig. 4), the cylindrical tip was used. To attach the wires, a hole of 1 mm diameter and 15 mm depth was drilled into the end of the tip down the axis of the model. A hole for an M3 grub screw was made into the side of the tip, 10 mm from the end, so that a wire could be inserted into the 1 mm hole and secured via the

grub screw. For the pulse tests, the impactor was used to strike the model on the flat end of the cylindrical tip.

Piezo film (polyvinylidene fluoride or PVDF film) was used as a strain sensor (Smith and Mee, 1996b). The gauge used in the tests was labelled *PF3* and was a 25 mm long piece of 28 μm thick piezo film wrapped around the stress bar with its most sensitive axis aligned with the axis of the bar. Such an arrangement provides bending compensation so that only axial strains are measured (Smith and Mee, 1996b). Gauge *PF3* was located 425 mm from the junction between the model and the stress bar. The gauge was connected to a PCB Model 462A Charge Amplifier that had a frequency response of 0.3 Hz to 180 kHz at -3 dB break points. PVDF film can be sensitive to changes in pressure. Whilst the sting was shielded from aerodynamic loads in the shock-tunnel tests, the gauge was further isolated from changes in pressure within the shielding by enclosing it in a sealed sleeve around the stress bar. In all tests, a 12-bit data-acquisition system, designed and built in-house, was used to record the strain and pressure signals at intervals of 5 μs .

In the tunnel tests, the model and stress bar were aligned with the flow so that only axial aerodynamic loads were present and the complete arrangement was free to move in the axial direction. The base of the cone was shielded from the flow to minimize any contribution of base pressure to the force on the cone. The shielding surrounds both the sting and the support threads, to protect them from experiencing any aerodynamic loads, as shown in Fig. 2. During the test period the model was able to move freely in the axial direction without touching the shielding. In the tunnel shots the Pitot pressure in the test section was measured simultaneously with the drag force measurements. The Pitot probe was set in line with the base of the cone but 75 mm from the axis of the cone. This meant that the Pitot probe was within the test core of the nozzle (where Pitot pressure varies by less than $\pm 5\%$; Overton and Mee, 1994) but was outside of the shock from the cone. Also, at that location, the bow shock from the probe does not strike the cone. All deconvolution calculations were done in the time domain using the extended conjugate gradient method outlined in Prost and Goutte (1984).

4.1 Dynamic calibration tests

The calibration tests employed three of the calibration techniques discussed in section 3; the two vertical calibration arrangements shown in Fig. 4, referred to as “hung-weight” calibrations (Fig. 4(a)) and “self-weight” calibrations (Fig. 4(b)), and pulse test calibrations, using the arrangement shown in Fig. 5. The vertical calibration tests were done prior to testing the model in the T4 shock tunnel and the pulse calibration tests were done after the shock tunnel tests, but while the model was still installed in the test section of the tunnel. The calibration tests are described first and typical results from each of the calibration techniques are shown. Then cross checks are

performed by deconvolving signals from one type of calibration test with impulse responses determined from the other calibration techniques.

4.1.1 Determination of the impulse response from a step input: Hung-weight test

For the hung-weight tests, the force balance/model arrangement was suspended from the downstream end of the stress bar via a loop of steel wire that passed through holes drilled through the stress bar 15 mm from its end. This wire loop was then attached to a steel frame mounted from the wall of the laboratory. The arrangement is shown schematically in Fig. 4(a). A mass of 4.23 ± 0.01 kg was suspended from the tip of the cone using stainless steel gauge 30 wire (0.3 mm diameter). This wire was cut within 10 mm of the tip of the model using standard, sharp wire cutters.

A sample step response obtained from such a test is shown in Fig. 6. The output signal is initially at zero with a sudden change occurring at 500 μs . In order to obtain this result, the data acquisition system was triggered using the sudden change in the level of the strain signal with a fixed number of pre-trigger samples. The actual time at which the load was removed from the tip is not time zero in the figure. However, this time can be estimated by considering the propagation of stress waves between the points of application of the load and measurement of the strain. This requires knowledge of the distance to the strain gauge from the tip of the model and the material of the structure between the tip and the gauge. For the present model, the first 25 mm of the stress wave’s path is through the steel tip of the model, the next 164 mm through the aluminium model and the final 425 mm through the brass stress bar. Taking the stress wave speeds in these three materials to be 5.2, 5.0 and 3.5 km/s respectively, the time taken for the first waves to reach the gauge will be approximately 160 μs . Thus, for this case, the cut time is at approximately 340 μs in Fig. 6.

The impulse response can be determined by differentiating this step response with respect to time, as described in section 3. To get the timing correct, the signal must first be shifted in time, in this case by -340 μs , and the resulting signal differentiated. This value of the time shift is appropriate for the present situation where the loading is due to a point load applied at the tip of the model. When an impulse response is required for deconvolving signals from a test in a wind tunnel, it could be argued that this time delay may not be appropriate. Aerodynamic forces will be distributed over the surface of the model and will not be concentrated at the tip. Thus when using an impulse response such as that determined from an hung-weight test, it may be suitable to determine the delay in wave propagation for some other reference point on the model. This will become important as the model size increases.

The performance of the force balance may be sensitive to the way in which the forces are distributed spatially and temporally over the model. Some simulations of these

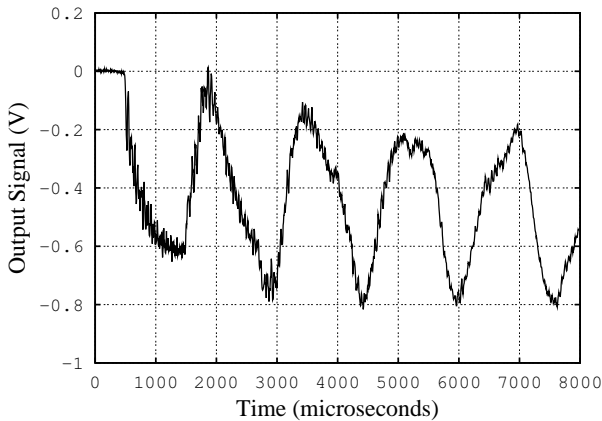


Fig. 6. Sample step response obtained by cutting a wire supporting a mass suspended from the tip of the model (Hung-weight test HW112).

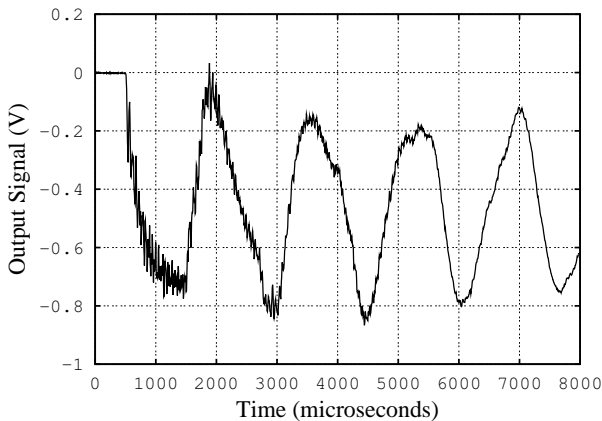


Fig. 7. Sample step response obtained by cutting a wire supporting the model vertically from its tip. (Self-weight test SW202)

effects on a long, conical model are considered in Tuttle *et al.* (1995), but distributed load impulse responses can also be obtained using the techniques considered in this paper. Since the arrangement is being modelled as a linear system, the results from several individual step response tests, with loads applied at different points on the model, can be superposed to infer the step response that would be obtained if the model had several weights hanging from these different points and the wires were cut simultaneously. Impulse responses from such distributed load step responses have been used for multiple-component stress-wave force-balances (e.g. Mee *et al.*, 1996; Smith *et al.*, 2001). The same principle can also be applied to pulse calibration tests to obtain distributed load impulse responses. It is also possible to model the temporal effects of changes in flow conditions convecting over the model with the flow by delaying the step responses for locations on the model downstream relative to from those upstream, see Tuttle *et al.* (1995).

4.1.2 Determination of the impulse response from a step input: Self-weight test

For the self-weight tests, the force balance/model arrangement was suspended from the tip of the model using stainless steel gauge 30 wire as shown in Fig. 4(b). The wire was cut within 10 mm of the tip of the model using wire cutters. The total mass of the model, force balance and cables being suspended by the wire was 4.94 ± 0.02 kg. A sample result from such a self-weight test is shown in Fig. 7. As for the hung-weight test, the output signal is initially zero and drops suddenly when the first stress waves reach the gauge location. There are two obvious differences between the signals in Figs. 6 and 7. Firstly, the level of the signal for the self-weight test is higher than that for the hung-weight test between times 500 and 1500 μs . This can be attributed to the different load levels being removed—the weight of a 4.94 kg mass compared with that of a 4.23 kg mass. The second difference occurs after the waves that have reflected from the downstream end of the stress bar reach the gauge measurement location (at approximately 1500 μs in Figs. 6 and 7). Note that the relative depth of the second trough compared with the first is more for the hung-weight test. As will be discussed in section 4.2, this is associated with the difference in the support condition at the end of the stress bar.

As for the hung-weight test, the time at which the wire was cut was determined by estimating the time for stress waves to travel from the tip of the model to the strain gauge location. The impulse response can be determined from this step response by shifting the signal in time, again in this case by about $-340 \mu\text{s}$, and differentiating the resulting signal with respect to time.

4.1.3 Determination of the impulse response from a pulse input

The pulse calibration tests were done after the tunnel shots but while the model was still installed in the test section of T4. The calibration tip was attached to the end of the cone in place of the sharp tip that had been used in the tunnel shots. The arrangement of the model and its suspension in the tunnel is shown schematically in Fig. 2. A PCB model 086C04 impulse force hammer was used to apply and measure the force pulse. The hammer uses a PCB ICP to condition the signal. The hammer was equipped with a steel tip. No extender was used.

A sample force pulse applied with the hammer in a pulse calibration test is shown in Fig. 8. Only a 600 μs window around the region of the force pulse is shown. It can be seen that the pulse is of about 240 μs duration and is approximately symmetrical in shape. There is a small amount of ringing of the transducer after the pulse and this decays to zero after about 1 ms. This ringing was larger in some pulse tests but the oscillations usually had a zero mean. At other times the signal is close to zero. The corresponding strain output signal from sensor *PF3* is shown in Fig. 9.

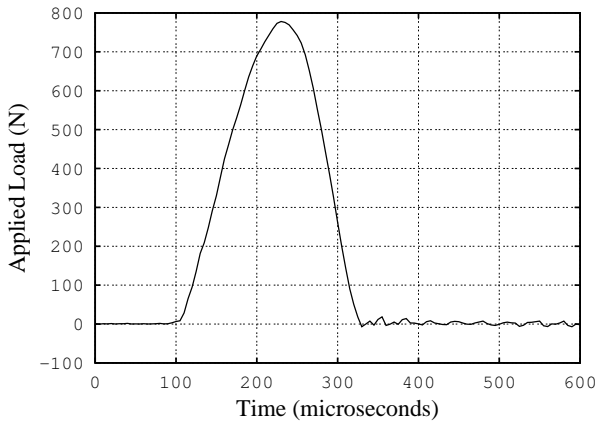


Fig. 8. Sample force pulse applied at the tip of the cone with the impulse force hammer (test 6274H7).

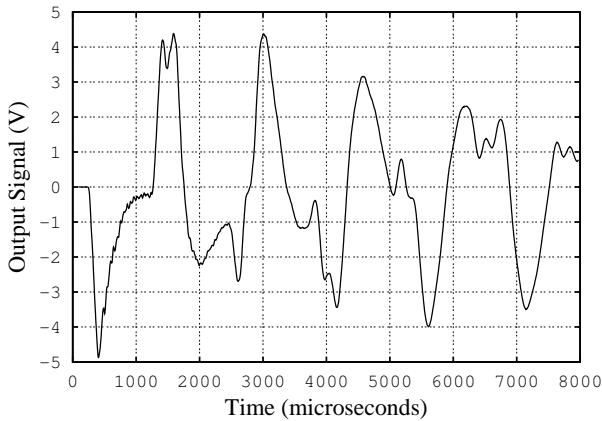


Fig. 9. Response of balance to the force pulse of Fig. 8.

Pulse calibrations have been found to be very sensitive to low frequency noise on the strain signals or small DC offsets in the pulse signal (Mee, 2002). It is very important to eliminate any low frequency noise (e.g. line noise) from the strain signal using standard noise-reduction techniques. The problem with small DC offsets in the hammer signal arises because the total impulse from a small, non-zero signal over a relatively long time can integrate to a significant impulse compared with the impulse applied during the relatively short impact period. It has been found that best results are obtained when the hammer signal is forced to be zero outside of the times during which the hammer and the model are in contact. With the present hammer and model the contact duration varied between 180 and 240 μs . A “modified” hammer signal was prepared for calibration test 6274H7; the hammer pulse was identified to occur between 90 and 330 μs in the plot of Fig. 8 and the signal was set to zero at other times.

From the output signal of Fig. 9 and the modified hammer pulse the impulse response of the system can be determined using the two methods outlined in section 3.2. To determine the impulse response by dividing the pulse response by the impulse applied by the hammer, the area under the force *vs* time curve for the hammer pulse must be determined. This has been done for the “modified” pulse

used here and the total impulse applied by the hammer is 0.101 Ns.

4.2 Cross-checks on calibration techniques

Four impulse response functions have been determined from the sample calibration tests. These impulse responses are numbered IR 1 to IR 4 and are formed from

1. the hung-weight test, HW112,
2. the self-weight test, SW202,
3. the hammer pulse test, 6274H7, by dividing the measured response by the area under the force *vs* time curve,
4. the hammer pulse test, 6274H7, by deconvolving the measured response with the hammer signal.

In determining the impulse responses and using them for deconvolution, it is appropriate to consider the effects of noise on the results and appropriate filtering of the signals. As noted, a 200 kHz sampling frequency was used for the data acquisition system for the impulse response calibration tests and for recording the shock tunnel results. For the type of signals expected in the shock tunnel tests, information up to frequencies of approximately 30 kHz is expected to be sufficient. There are many different types of filters that could be used to filter out higher frequency noise. Moving-average filters, that are simple to implement and use, have been found to be adequate for filtering the type of signals obtained using stress wave force balances. For these present tests, a 30 μs moving-average filter (a six-point filter for the current sampling rate) has been chosen.

In order to determine impulse responses IR 1, IR 2 and IR 4, the measured strain signals were first processed with a 30 μs moving-average filter. The impulse responses for case 3 will have a frequency response set by the duration of the pulse applied. Using this impulse response, it would not be possible to obtain information about frequencies as high as 30 kHz. So a longer-duration moving-average filter is necessary for this impulse response. Testing indicates that a moving-average filter of length about half the duration of the pulse is appropriate for the impulse responses determined by dividing the pulse response signal by the impulse of the impact. To determine impulse response IR 3, a 120 μs moving-average filter has been used.

These four impulse responses have then been used to deconvolve the step response obtained from another self-weight test, test SW203. The response from a self-weight test has been chosen as the test case for deconvolution because it has the same, free-end condition at the downstream end of the stress bar as in the shock tunnel shots. Also, as is confirmed by deconvolution with impulse response IR 4, the rise time for the step is short.

The results from the four deconvolutions are presented in Fig. 10. The deconvolved signals obtained using impulse responses IR 1, IR 2 and IR 4 were then processed with a 30 μs moving-average filter and that for impulse response IR 3 was processed with a 120 μs moving-average filter.

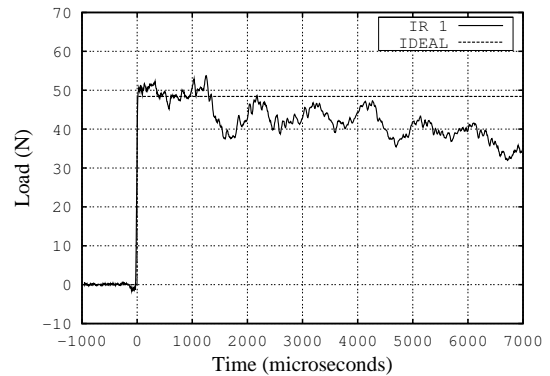
The timescale has been adjusted so that the weight is cut at time zero.

The result for the impulse response derived from the hung-weight test, Fig. 10(a), shows the effect of the wrong end condition at the downstream end of the stress bar. The recovered load is at approximately the correct level (48.4 N) for just over one millisecond after the wire was cut but then it starts to deviate from the correct value. The signal should be correct until the first reflection of stress waves from the downstream end of the bar reach the strain measurement location. Until that time there can be no effect of the end condition on the result. For the present arrangement this time is estimated to be 1.3 ms using the wave speeds in the materials of the model and stress bar. This time agrees well with the deviation from the correct load in the figure. As there are further reflections up and down the force balance, the deconvolved signal continues to deviate from the correct load value. The recovered signal in the first 1.3 ms is not as good as for the other cases shown. This is attributed to a poorer signal-to-noise ratio and not as clean a cutting of the wire for test HW112—note in Fig. 6 that, before the rapid change in strain, the strain output signal starts to deviate from horizontal. Despite this, the mean recovered signal during the first 1.3 ms after the cut is still within 2.5% of the true level.

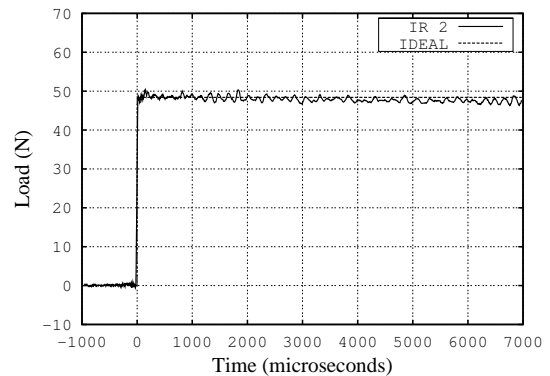
The result for impulse response IR 2, presented in Fig. 10(b), shows a good recovery of the applied load. Towards the end of the record, the recovered signal is approximately 2% lower than the true level. The signal rise time (10–90%) is approximately 30 μ s. This corresponds to the duration of the moving-average filter that was applied to reduce noise.

The best recovery of the load for the impulse responses determined from the pulse calibration test is for case IR 4, where the impulse response was found by deconvolving the measured strain signal with the hammer pulse signal, Fig. 10(d). Two important points are drawn from this result. Firstly, the signal level is recovered well over the entire period considered, indicating that it is possible to obtain a good estimate of the impulse response by using this pulse calibration technique. Secondly, the recovered signal is seen to rise rapidly to the correct level, indicating that the method of obtaining a step response by cutting a fine wire attaching a load to the model gives a rapid removal of the load. This is illustrated more clearly in Fig. 11 where the first 100 μ s of this signal either side of the cut is shown. There is some noise on the signal, but it can be seen that it rises within approximately the 30 μ s that was used for the moving-average filter. It can also be seen that there is about a 15 μ s delay in the signal, indicating that the time taken for waves to travel from the tip of the cone to the strain measurement is overestimated by about 10% in the self-weight test. So both the self-weight and the pulse calibration techniques are suitable for obtaining the impulse response for a system such as that used here.

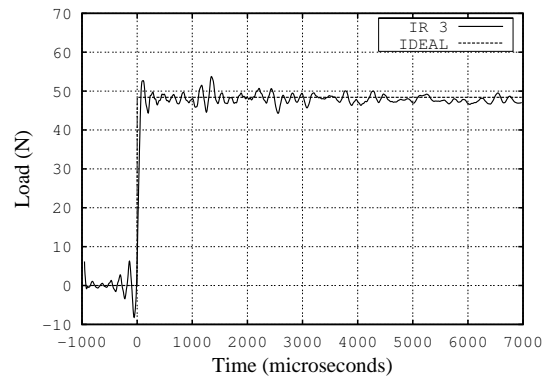
A reasonable recovery of the step is obtained using the impulse response determined by dividing the pulse response by the applied impulse (see Fig. 10(c)). The expected drop in response time of the balance is apparent



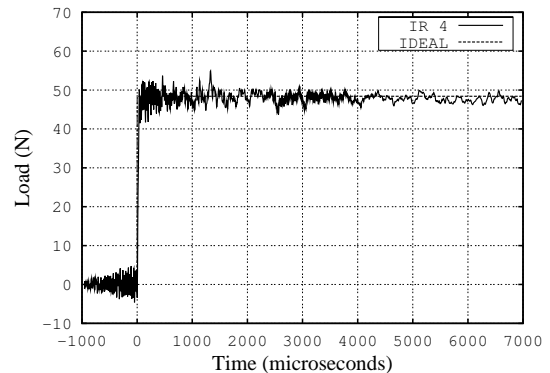
(a) IR 1, from HW112.



(b) IR 2, from SW202.



(c) IR 3, from 6274H7, area method.



(d) IR 4, from 6274H7, deconvolution method.

Fig. 10. Step response of test SW203 deconvolved with the four impulse responses.

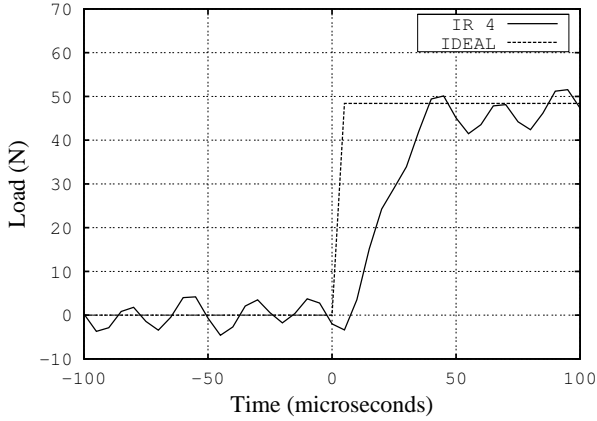


Fig. 11. The first 100 μs either side of the cut for the result in Fig. 10(d).

and there is some ringing either side of the step. There is also some ringing induced at about 1.3 ms after the step. This is attributed to rapid changes in the strain signal as the primary reflection of the stress waves due to the applied load return to the gauge location after reflecting from the downstream end of the stress bar. Despite some loss in frequency response, the load level is well recovered.

The results show that any of the four calibration techniques can recover the applied load to within 2.5%. The response time for IR 3 is longer than for the other techniques and IR 1 can only be used to infer load levels for the first 1.3 ms. The uncertainty in force measurement using the techniques outlined here is estimated to be $\pm 3\%$.

5 Shock-tunnel tests

The model used in the bench tests was tested at four conditions in the T4 shock tunnel. The conditions in the nozzle supply region were determined from the shock tube filling conditions and the measured shock speed using the code ESTC (McIntosh, 1970). The conditions in the test section of the tunnel were determined using the nozzle supply conditions and the nozzle shape using the code NENZF (Lordi *et al.*, 1966). The flow was expanded until the ratio of Pitot pressure to nozzle supply pressure, calculated by NENZF, matched the mean value during the test period of the measured ratio of Pitot pressure to nozzle supply pressure. For shot 6271, NENZF was run in the mode where equilibrium chemistry was used in the nozzle expansion. For the other cases, non-equilibrium chemistry was used. The test conditions are shown in Table 1. The subscript ∞ refers to conditions of the freestream flow in the test section.

The strain signal measured for shot 6271 is shown in Fig. 12. This strain signal has been deconvolved with each of the four impulse responses determined from the calibration tests in section 4.2. Prior to deconvolution, the strain signal was filtered with a 30 μs moving-average filter for the cases where IR 1, IR 2 and IR 4 were used. For impulse response IR 3, the strain signal was passed through a

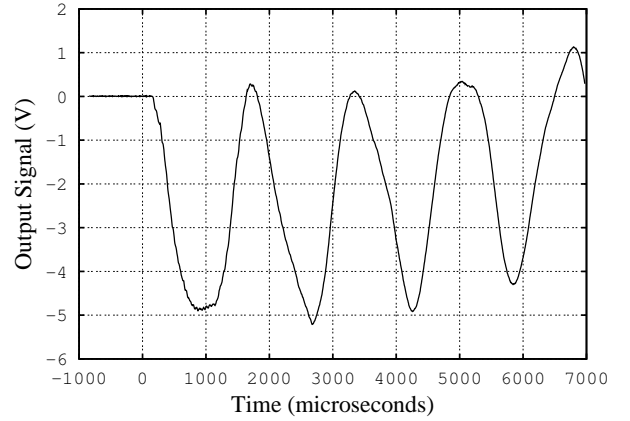
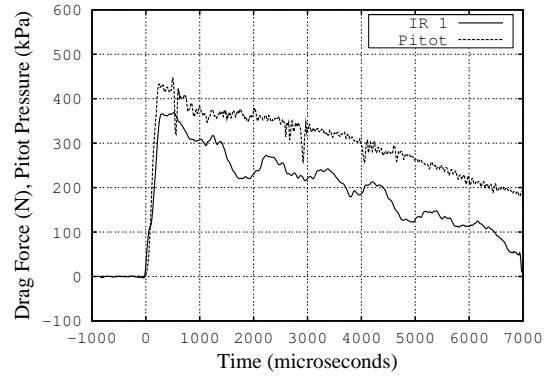
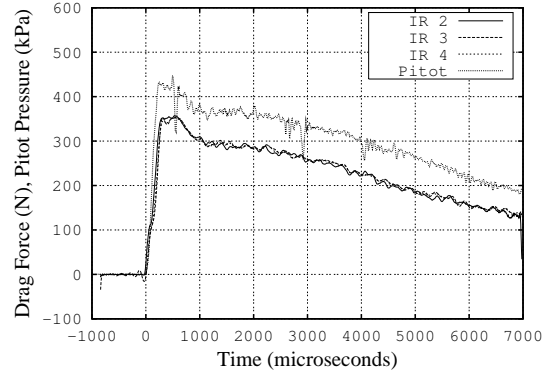


Fig. 12. Strain signal for shot 6271.



(a) IR 1, from HW112.



(b) IR 2, from SW202; IR 3, from 6274H7, area method; IR 4, from 6274H7, deconvolution method.

Fig. 13. The strain signal of shot 6271 deconvolved with the four impulse responses.

120 μs moving-average filter prior to deconvolution, as discussed in section 4.2. After deconvolution, the same length moving-average filters were passed through the data and the final results are shown in Fig. 13.

There are some expected similarities between the deconvolved drag signals in Fig. 13 and the signals from the step response test presented in Fig. 10. The force signal for shot 6271, determined using the impulse response that was obtained from the hung-weight test (IR 1), shows large, low frequency oscillations beyond about 1.3 ms af-

Table 1. Flow conditions for the T4 shots.

Shot	Nozzle Supply enthalpy MJ/kg	Nozzle supply pressure MPa	M_∞	v_∞ m/s	p_∞ kPa	ρ_∞ kg/m ³	T_∞ K	γ
6271	3.4	28	6.5	2470	6.6	0.064	360	1.4
6272	9.7	4.7	5.9	3760	1.4	0.0046	970	1.37
6273	11.1	31	5.4	4110	11.6	0.026	1480	1.33
6274	8.2	32	5.7	3650	10.1	0.033	1050	1.34

ter flow arrival. This again is attributed to the different end condition between the calibration test and the tunnel shot. The signal obtained using IR3 in Fig. 13(b) has small oscillations that are again attributed to the poorer frequency response associated with the calibration method used. However, the oscillations are much smaller than for the case of the step response result in Fig. 10(c).

The three calibration techniques recommended for deconvolving tunnel signals such as that for shot 6271 are the self-weight test (IR 2), the pulse test with the impulse response found by dividing the response by the area under the pulse (IR 3) and the pulse test with the impulse response found by deconvolving the response with the pulse signal (IR 4). The direct comparison of the results obtained using these three impulse responses, shown in Fig. 13(b), indicates very good agreement over the entire record shown.

Figure 13 also shows the time record of the Pitot pressure, measured in the test section, simultaneously with the drag force. It is straightforward to show that the time record of drag coefficient, C_D , during a test in a hypersonic flow can be found from the measured time records of drag force, D , and Pitot pressure, p_{Pit} , in the form (Mee, 2002)

$$C_D \approx \text{const.} \frac{D}{A p_{Pit}}, \quad (12)$$

where the constant depends on the ratio of specific heats of the test gas and A is reference area for the drag coefficient. For the present model, A is taken as the base area of the cone, $7.5 \times 10^{-3} \text{ m}^2$. Thus, for a constant drag coefficient, the drag force and Pitot pressure should have similar histories. Note that the Pitot pressure was measured in line with the base of the cone while the forces on the cone are referenced to the tip of the model (because the forces were applied at the tip of the cone in the calibration tests). For shot 6271, the flow speed was 2470 m/s. Given the cone length of 182 mm, it will take the flow approximately $75 \mu\text{s}$ to pass from the tip of the cone to the base. To account for this, the Pitot pressure has been shifted forward in time by $75 \mu\text{s}$ relative to the drag force signal in the plots in Fig. 13. It can be seen that the drag force signals follow the changes in Pitot pressure for the times shown, including the initial overshoot at the start and the decrease in pressure at later times.

Based on mass-spectrometry measurements in the T4 shock tunnel (Skinner, 1994) and results from a driver-gas detector (Paull, 1996), the level of contamination of the test gas by the driver gas should be less than 7.5% for the

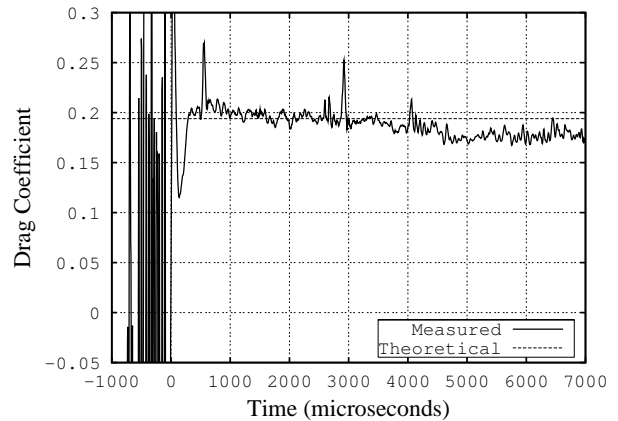


Fig. 14. The drag coefficient, C_D , for shot 6271. D determined using IR 4.

first 4 to 5 ms after flow arrival at the conditions of shot 6271. It is apparent that the tuning of the conditions for the shot (Jacobs et al., 1993) sees the pressure levels start to decrease earlier than this.

The drag force signal obtained using IR 4 has been used with eq. (12) to produce the inferred drag coefficient shown in Fig. 14. It can be seen that, after an initial flow establishment period, the drag coefficient is approximately steady between 1 and 3 ms after flow arrival. At later times the decreasing drag coefficient is attributed to a slow increase in the pressure within the shielding that contains the stress bar. This pressure acts on the base of the cone and decreases the net drag force on the cone. Measurements of pressure in the base region were attempted and indicated that the base pressure increased to approximately 3 kPa, 7 ms after flow arrival for shot 6271 which would account for the decrease in C_D observed in Fig. 14. However, reliable compensation for drag force time record using these measurements was not possible because of the low levels of pressure and acceleration sensitivity of the gauges used.

Shown also in Fig. 14 is a theoretical prediction of the drag coefficient for the cone at this condition. This prediction is based on the pressure drag on the cone surface, determined from the surface pressure on the cone based on the theory of Taylor and Maccoll (1932). Skin friction drag is taken into account using the conditions on the cone surface from Taylor and Maccoll (1932) and assuming a laminar boundary layer. The distribution of skin-friction coefficient is based on the reference temperature method in eq. (7.45b) of White (1974). The base pressure on the

cone has been assumed to be zero. The skin friction calculations are based on the flow conditions during the test time, 1 to 2 ms after flow arrival. Taking the uncertainty in Pitot pressure in the test section to be $\pm 5\%$ and other uncertainties in conditions as given in Mee (1993), the uncertainty in the theoretical drag coefficient for this condition is estimated to be $\pm 4\%$. Apart from some spikes associated with noise on the Pitot pressure signal, the experimental results agree with theoretical values to within this uncertainty limit for the first 4 ms. The measured results deviate from the prediction at later times as the base pressure increases and the test flow becomes contaminated with driver gas.

The agreement between the force signals for shot 6271 obtained using impulse responses IR 2, IR 3 and IR 4 (see Fig. 13b) is in line with the estimated accuracy of $\pm 3\%$ in force measurement using the different calibration techniques. It should be noted that single point-load calibration techniques, such as those used here, may not be suitable for more complex or larger models (Tuttle *et al.*, 1995). Also, calibrations from loads applied at more than one location are required for multiple-component balances (Mee *et al.*, 1996).

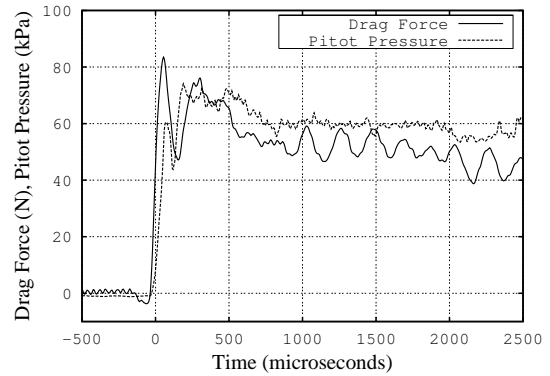
The other three shock tunnel tests were performed at higher enthalpy conditions (refer to Table 1). At higher enthalpy, the flow establishment time is shorter but the duration of the test flow is terminated earlier by contamination by the driver gas than for shot 6271. Contamination times are estimated to be around 1.5 to 2.0 ms after flow start for shots 6272, 6273 and 6274 (Paull, 1996). Drag forces obtained for these shots using impulse response IR 4 are shown in Fig. 15. The results are shown for only the first 2.5 ms after flow arrival because of the shorter test times. Shown again are the histories of Pitot pressure. After a flow establishment time and prior to contamination, the drag force can be seen to follow the history of Pitot pressure. The higher noise levels in the result for shot 6272 are attributed to the poorer signal-to-noise ratio for the lower level of drag at that condition.

An example of the drag coefficient inferred from the drag force and Pitot pressure measurements for a higher-enthalpy condition, test 6274, is shown in Fig. 16. As for the result at the lower enthalpy shown in Fig. 14, a steady signal is obtained during the test period. The measured drag coefficient for shot 6274 is within 5% of the theoretical value. This is in line with the estimated uncertainty in measured drag force of $\pm 3\%$ and uncertainty in the theoretical drag coefficient of $\pm 4\%$.

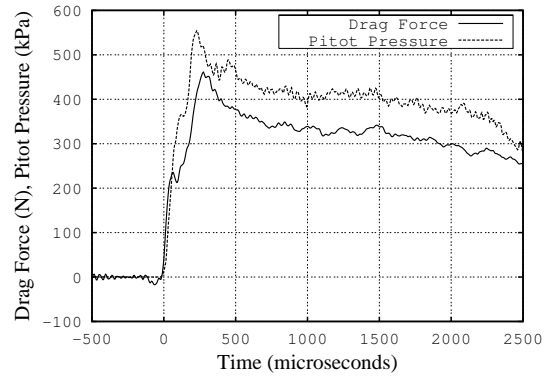
6 Conclusions

Different techniques for the dynamic calibration of stress wave force balances have been considered in this paper. It has been shown that one or more calibration techniques may be suitable for a particular force measurement application.

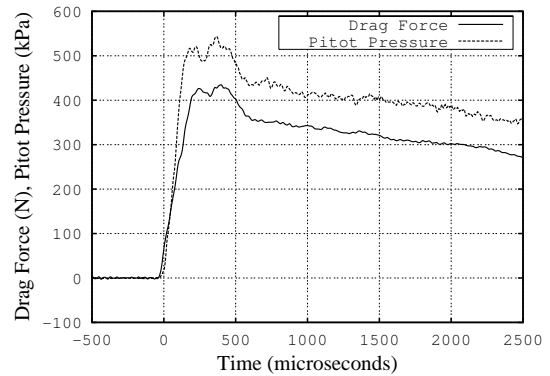
For short test times, hung-weight calibration techniques can be used for freely suspended force balances. However,



(a) Shot 6272.



(b) Shot 6273.



(c) Shot 6274

Fig. 15. The deconvolved drag force signals (using IR 4) and Pitot pressure signals for the higher enthalpy shots.

if the supporting arrangement for the force balance is different between the calibration tests and experiments in a wind tunnel, the effect of the supporting arrangement must be considered. The derived impulse response may be valid for a limited period of time in such cases. Free-end calibration techniques, such as self-weight or pulse tests are appropriate for cases where longer duration impulse responses are required.

The technique of cutting a fine wire either supporting a weight or supporting the model and force-balance arrangement can be used to apply a step change in load to the model. The results of deconvolving the strain signals from self-weight tests with impulse responses derived from pulse calibrations indicates that the wire cutting technique

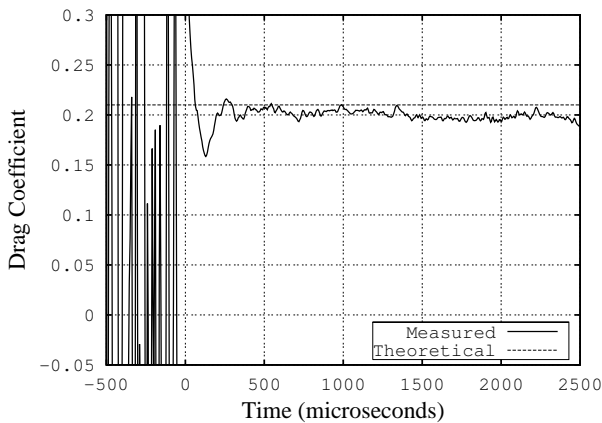


Fig. 16. The drag coefficient, C_D , for shot 6274. D determined using IR 4.

leads to a step change in load in less than $30 \mu\text{s}$ - the limit of the resolution obtained for the filtering techniques used in this article.

For cases where a high frequency response is not required, the impulse response can be determined from a pulse calibration by dividing the strain response signal by the magnitude of the impulse applied in the test. An impulse response with a higher frequency response can be obtained from a pulse test if the strain response signal is deconvolved with the measured applied pulse signal.

Care needs to be taken when using pulse calibration techniques to determine impulse responses. Small errors in either the pulse signal or the strain signal can lead to large errors in the impulse response at large times. Cross-checking the results from impulse responses derived using different calibration techniques enables any errors in the calibration procedure or processing to be clearly identified. It is recommended that such cross checks be used, where possible, to minimize potential errors in the calibration.

For models, instrumentation and calibration techniques of the type used in this study, the accuracy of force measurements is estimated to be $\pm 3\%$.

Acknowledgement. This work was performed under grants supported by the Australian Research Council. Thanks go to Tony Gardner for assistance in running the T4 shock tunnel. Thanks also go to Prof. KPJ Reddy of the Indian Institute of Science for the opportunity to complete analysis for this paper while the author was on study leave at IISc.

References

- Bernstein L (1975) Force measurements in short-duration hypersonic facilities. AGARDograph 214
- Carbonaro M (1993) Aerodynamic force measurements in the VKI longshot hypersonic facility. In *New Trends in Instrumentation for Hypersonic Research* (ed. A. Boutier) Dordrecht, The Netherlands: Kluwer. 317–325
- Daniel WJT, Mee DJ (1995) Finite element modelling of a three-component force balance for hypersonic flows. *Computers and Structures* **54**(1):35–48

- Dieulesaint E, Royer D (1980) *Elastic waves in solids—Applications to signal processing*. Chichester: Wiley.
- Doebelin EO (1980) *System Modeling and Response: Theoretical and Experimental Approaches*. New York: John Wiley and Sons.
- Jacobs PA, Morgan RG, Stalker RJ, Mee DJ (1993) Use of Argon-Helium driver-gas mixtures in the T4 shock tunnel. In *Shock Waves @ Marseille I*, R Brun and LZ Dumitrescu (Eds.). Springer, Berlin, 263–268
- Jessen C, Groenig H (1989) A new principle for a short-duration six component balance. *Experiments in Fluids* **8**(3–4):231–233
- Joshi MV, Reddy MN (1986) Aerodynamic force measurements over missile configurations in IISc shock tunnel at $M_\infty = 5.5$. *Experiments in Fluids* **4**(6):338–340
- Lordi JA, Mates RE, Moselle JR (1966) Computer program for numerical solution of nonequilibrium expansion of reacting gas mixtures. NASA Contractor Report CR-472
- McConnell KG (1995) *Vibration testing: theory and practice*. Wiley, New York
- McConnell KG, Abdelhamid MK (1987) On the dynamic calibration of measurement systems for use in modal analysis. *Journal of Modal analysis* **2**(3):121–127
- McIntosh MK (1970) Computer programmes for supersonic real gas dynamics. Department of Supply, Australian Defence Scientific Service, Weapons Research Establishment. WRE-TN-180
- Mee DJ (1993) Uncertainty analysis of conditions in the test section of the T4 shock tunnel. Department of Mechanical Engineering, The University of Queensland. Research Report 4/93
- Mee DJ (2002) Dynamic calibration of force balances. Department of Mechanical Engineering, The University of Queensland. Research Report 2002/6
- Mee DJ, Daniel WJT, Simmons JM (1996) Three-component force balance for flows of millisecond duration. *AIAA Journal* **34**(3):590–595
- Naumann KW, Ende H, Mathieu G, George A (1993) Millisecond aerodynamic force measurement with side-jet model in the ISL shock tunnel. *AIAA Journal* **31**(6):1068–1074
- Overton S, Mee DJ (1994) T4's M5 and M8 nozzle Pitot rake survey. Proceedings of the 4th International Workshop on Shock Tube Technology. A. Paull (Ed.) Brisbane 20–23 September 1994
- Paull A (1996) A simple shock tunnel driver gas detector. *Shock Waves* **6**(5):309–312
- Paull A, Stalker RJ, Mee DJ (1995) Experiments on supersonic combustion ramjet propulsion in a shock tunnel. *Journal of Fluid Mechanics* **296**:159–183
- Prost R, Goutte R (1984) Discrete constrained iterative deconvolution algorithms with optimized rate of convergence. *Signal Processing* **7**(3):209–230
- Reed RP (1998) Convolution and deconvolution in measurement and control: Part 7—system transient response characterization for convolution and deconvolution. *Measurements and Control* **189**:69–83
- Sanderson SR, Simmons JM (1991) Drag balances for hypervelocity impulse facilities. *AIAA Journal* **29**(12):2185–2191
- Skinner KA (1994) Mass spectrometry in shock tunnel experiments of hypersonic combustion. PhD thesis, The University of Queensland.
- Smith AL, Mee DJ (1996a) Drag measurements in a hypervelocity expansion tube. *Shock Waves* **6**(3):161–166

- Smith AL, Mee DJ (1996b) Dynamic strain measurement using piezoelectric polymer film. *Journal of Strain Analysis for Engineering Design* **31**(6):463–465
- Smith AL, Mee DJ, Daniel WJT, Shimoda T (2001) Design, modelling and analysis of a six-component force balance for hypervelocity wind tunnel testing. *Computers and Structures* **79**(11):1077–1088
- Taylor GI, Maccoll JW (1932) The air pressure on a cone moving at high speed. *Proceedings of the Royal Society (London) Series A* **139**:278–297.
- Tuttle SL, Mee DJ, Simmons JM (1995) Drag measurements at Mach 5 using a stress wave force balance. *Experiments in Fluids* **19**(5):336–341
- White FM (1974) *Viscous Fluid Flow*. New York: McGraw-Hill